# From closed-boundary to single-sided homogeneous Green's function representations

Wapenaar, Kees; van der Neut, Joost; Thorbecke, Jan Willem; Slob, Evert; Singh, Satyan

**DOI**
10.1190/segam2016-13965149.1

**Publication date**
2016

**Document Version**
Accepted author manuscript

**Published in**
SEG Technical Program Expanded Abstracts 2016

# From closed-boundary to single-sided homogeneous Green's function representations

*Kees Wapenaar*, Joost van der Neut, Jan Thorbecke and Evert Slob, Delft University of Technology;*
*Satyan Singh, Colorado School of Mines*

## SUMMARY

The homogeneous Green's function (i.e., the Green's function and its time-reversed counterpart) plays an important role in optical, acoustic and seismic holography, in inverse scattering methods, in the field of time-reversal acoustics, in reverse-time migration and in seismic interferometry. Starting with the classical closed-boundary representation of the homogeneous Green's function, we modify the configuration to two parallel boundaries. We discuss step-by-step a process that eliminates the integral along the lower boundary. This leads to a single-sided representation of the homogeneous Green's function. Apart from imaging, we foresee interesting applications in inverse scattering, time-reversal acoustics, seismic interferometry, passive source imaging, etc.

## INTRODUCTION

The homogeneous Green's function plays an important role in optical, acoustic and seismic holography (Porter, 1970; Maynard et al., 1985; Wu and Toksöz, 1987; Lindsey and Braun, 2004), in linear inverse source problems and inverse scattering methods (Porter and Devaney, 1982; Oristaglio, 1989), in the field of time-reversal acoustics (Fink, 1997, 2008), in reverse-time migration (McMechan, 1983; Esmersoy and Oristaglio, 1988) and in seismic interferometry (Wapenaar, 2003; Derode et al., 2003; Weaver and Lobkis, 2004). The homogeneous Green's function is formed by a combination of the causal Green's function and its time-reversed version. An exact integral representation exists, but it is expressed in terms of a closed boundary integral. Here we explain in detail with numerical examples how the closed boundary integral can be transformed into an open integral, which thus leads to a single-sided integral representation of the homogeneous Green's function (Wapenaar et al., 2016). This single-sided representation has interesting applications in the fields mentioned above.

## THE HOMOGENEOUS GREEN'S FUNCTION

Consider a Green's function $G(\mathbf{x},\mathbf{x}_B,t)$, defined as the response to an impulsive source of volume injection rate at $\mathbf{x}_B$. It is the causal solution of the acoustic wave equation with a source term $-\delta(\mathbf{x}-\mathbf{x}_B)\partial_t\delta(t)$ on the right-hand side. For a lossless medium the wave equation is symmetric in time, except for the source term, which is antisymmetric in time. Hence, the time-reversed Green's function $G(\mathbf{x},\mathbf{x}_B,-t)$ obeys the same wave equation, but with an opposite source term $+\delta(\mathbf{x}-\mathbf{x}_B)\partial_t\delta(t)$. The sum of the Green's function and its time-reversal, i.e., $G_{\rm h}(\mathbf{x},\mathbf{x}_B,t)=G(\mathbf{x},\mathbf{x}_B,t)+G(\mathbf{x},\mathbf{x}_B,-t)$ also obeys the same wave equation, but with the source terms cancelling each other. Since in this case the right-hand side of the wave equation is zero, we speak of a homogeneous equation, and we call its solution $G_{\rm h}(\mathbf{x},\mathbf{x}_B,t)$ the homogeneous Green's function (not to be confused with the Green's function for a homogeneous medium). In the frequency domain, a representation for the homogeneous Green's function reads (Porter, 1970; Oristaglio, 1989; Wapenaar et al., 2005)

$$G_{\rm h}(\mathbf{x}_A,\mathbf{x}_B,\omega)=\oint_{\partial\mathbb{D}}\frac{-1}{j\omega\rho(\mathbf{x})}\{G^*(\mathbf{x},\mathbf{x}_A,\omega)\partial_i G(\mathbf{x},\mathbf{x}_B,\omega) -\partial_i G^*(\mathbf{x},\mathbf{x}_A,\omega)G(\mathbf{x},\mathbf{x}_B,\omega)\}n_i{\rm d}^2\mathbf{x}, \quad (1)$$

where $\omega$ denotes angular frequency, $\rho$ mass density, $j$ the imaginary unit and $*$ complex conjugation. $\partial\mathbb{D}$ is a closed boundary with outward pointing normal vector $(n_1,n_2,n_3)$, enclosing a domain $\mathbb{D}$, and $\mathbf{x}_A$ and $\mathbf{x}_B$ are the coordinate vectors of two points inside $\partial\mathbb{D}$, see Figure 1(a). Equation (1) is exact and thus accounts for all orders of multiple scattering inside and outside domain $\mathbb{D}$.

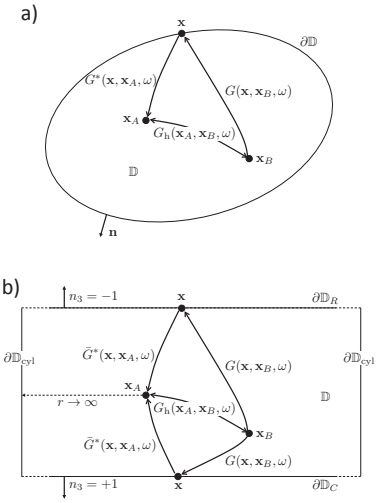


Figure 1: *(a) Configuration for the homogeneous Green's function representation (equation 1). The rays in this figure represent the full responses between the source and receiver points, including multiple scattering. (b) Configuration for the modified representation. The integral along $\partial\mathbb{D}_{\rm cyl}$ vansihes. When the integral along $\partial\mathbb{D}_C$ vanishes as well, a single-sided representation remains.*

For the configuration of Figure 1(b), we modify equation (1) as follows

$$G(\mathbf{x}_A,\mathbf{x}_B,\omega)+\bar{G}^*(\mathbf{x}_B,\mathbf{x}_A,\omega) \quad (2)$$
$$=\int_{\partial\mathbb{D}_R}\frac{1}{j\omega\rho}\{\bar{G}_A^*\partial_3 G_B-\partial_3\bar{G}_A^* G_B\}{\rm d}^2\mathbf{x}$$
$$-\int_{\partial\mathbb{D}_C}\frac{1}{j\omega\rho}\{\bar{G}_A^*\partial_3 G_B-\partial_3\bar{G}_A^* G_B\}{\rm d}^2\mathbf{x},$$

where $\partial\mathbb{D}_R$ and $\partial\mathbb{D}_C$ are two infinite horizontal boundaries. The contribution of the integral along the cylindrical boundary $\partial\mathbb{D}_{\text{cyl}}$ vanishes. $\bar{G}_A$ and $G_B$ are short-hand notations for $\bar{G}(\mathbf{x},\mathbf{x}_A,\omega)$ and $G(\mathbf{x},\mathbf{x}_B,\omega)$, respectively. We replaced $G_A$ by a Green's function $\bar{G}_A$ in a reference medium, which is identical to the actual medium below $\partial\mathbb{D}_R$, but homogeneous at and above $\partial\mathbb{D}_R$. To arrive at a single-sided integral representation, we have to eliminate the integral along the lower boundary $\partial\mathbb{D}_C$. This is the subject of the next section.

## AN AUXILIARY FUNCTION

We introduce an auxiliary function $\Gamma(\mathbf{x},\omega)$ which we subtract from the Green's function, according to

$$\bar{G}(\mathbf{x},\mathbf{x}_A,\omega) \rightarrow \bar{G}(\mathbf{x},\mathbf{x}_A,\omega) - \Gamma(\mathbf{x},\omega). \tag{3}$$

As long as $\Gamma(\mathbf{x},\omega)$ obeys the same wave equation in $\mathbb{D}$ as $\bar{G}(\mathbf{x},\mathbf{x}_A,\omega)$, but without a source term, we can make this replacement in equation (2), hence,

$$\begin{aligned} &G(\mathbf{x}_A,\mathbf{x}_B,\omega) + \{\bar{G}(\mathbf{x}_B,\mathbf{x}_A,\omega) - \Gamma(\mathbf{x}_B,\omega)\}^* \qquad (4)\\ &= \int_{\partial\mathbb{D}_R} \frac{1}{j\omega\rho}\{(\bar{G}_A-\Gamma)^*\partial_3 G_B - \partial_3(\bar{G}_A-\Gamma)^* G_B\}\mathrm{d}^2\mathbf{x}\\ &- \int_{\partial\mathbb{D}_C} \frac{1}{j\omega\rho}\{(\bar{G}_A-\Gamma)^*\partial_3 G_B - \partial_3(\bar{G}_A-\Gamma)^* G_B\}\mathrm{d}^2\mathbf{x}. \end{aligned}$$

We search for a function $\Gamma$, such that both $\bar{G}_A-\Gamma$ and $\partial_3(\bar{G}_A-\Gamma)$ vanish on $\partial\mathbb{D}_C$ (these are the Dirichlet and Neumann boundary conditions, which together are known as the Cauchy boundary condition, hence the subscript $C$ in $\partial\mathbb{D}_C$). Introducing auxiliary functions is a common approach to manipulate the boundary conditions (Morse and Feshbach, 1953; Berkhout, 1982). For the integral in equation (4) this was previously proposed by Weglein et al. (2011), but solved only for some special cases. Recently we proposed a more general way to find a $\Gamma$ that obeys both boundary conditions for arbitrary inhomogeneous media (Wapenaar et al., 2016). Here we explain this method in more detail and illustrate it step by step with a numerical example. Although the numerical example is 1D, the proposed approach holds for 3D inhomogeneous media.

We consider a horizontally layered medium, with interfaces at $z = 300$, 600 and 900 m. The propagation velocities in the layers are 1500, 1950, 2000 and 2300 m/s and the mass densities are 1000, 4500, 1400 and 1600 kg/m$^3$, respectively. A Green's source is defined at $z_A = 800$ m. The 1D time-domain Green's function $\bar{G}(z,z_A,t)$ is shown in a VSP-like display in Figure 2. The red dot denotes the source, the red lines the direct arrivals. The traces in the top and bottom panels are the responses at $z_R = 0$ and $z_C = 1175$m, respectively, denoted by the blue dots. The auxiliary function $\Gamma(z,t)$ should be defined such that at $z_C$ it cancels the Green's function $\bar{G}(z_C,z_A,t)$ (i.e., the trace in the bottom panel of Figure 2). The focusing functions, introduced earlier for Marchenko imaging (Broggini and Snieder, 2012; Wapenaar et al., 2013; Slob et al., 2014; van der Neut et al., 2015), can generate such a function. The top panel in Figure 3 shows the focusing function $f_1^+(z_R,z_A,t)$, which is emitted from $z_R = 0$ into the medium. The VSP-like panel shows the evolution of this focusing function through the

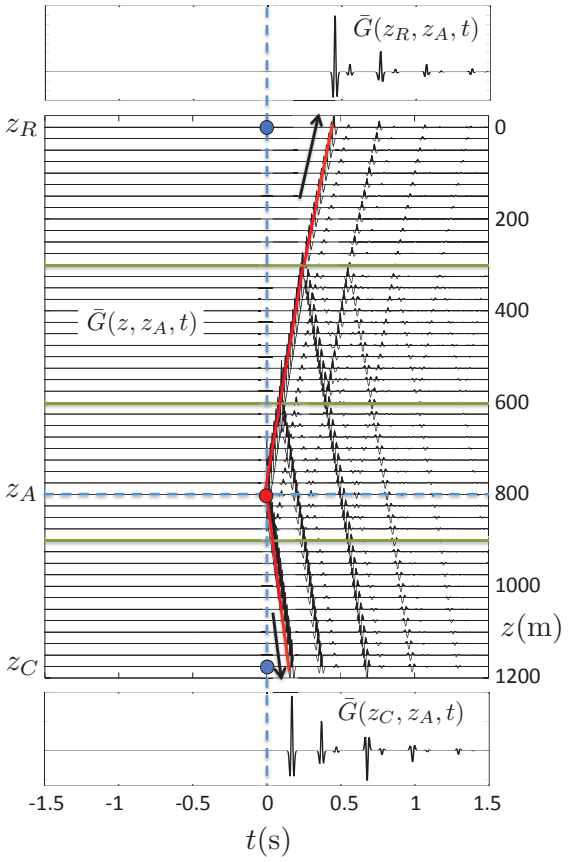


Figure 2: *The Green's function $\bar{G}(z,z_A,t)$ in a horizontally layered medium. In equation (4) we need an auxiliary function $\Gamma(z,t)$ which, at $z_C = 1175$ m, cancels this Green's function.*

medium (left of the red lines). The field focuses at $z_A = 800$ m (the yellow dot). The focused field at $z_A$ acts as a virtual source for downgoing waves, of which the response is denoted as $\bar{G}^{p,+}(z,z_A,t)$ (where the second superscript, $+$, denotes the downgoing source at $z_A$, and the first superscript, $p$, the total pressure field at $z$). This response is shown right of the red lines in Figure 3. The response at $z_C$, denoted by the blue dot, is shown in the lower panel of Figure 3. It contains part of the events of $\bar{G}(z_C,z_A,t)$ in Figure 2. The events still missing in Figure 3 are those caused by the upward radiating part of the source at the red dot in Figure 2. We now discuss how this remaining part of $\bar{G}(z_C,z_A,t)$ can be recovered by another focusing function. Consider again the focusing function $f_1^+(z,z_A,t)$ in Figure 3. Before reaching the focus, a part of this focusing function is reflected upward and is called $f_1^-(z,z_A,t)$. At $z = z_R$ we reverse this field in time and change its polarity, yielding $-f_1^-(z_R,z_A,-t)$. Figure 4 shows the emission of this new focusing function into the medium. Left of the red lines, its response is $-f_1^-(z,z_A,-t) - f_1^+(z,z_A,-t)$. The response right of the red lines apparently originates from a source for upgoing waves at the yellow dot at $z_A$, hence, this response is denoted as $\bar{G}^{p,-}(z,z_A,t)$ (where the second superscript, $-$, denotes the upgoing source at $z_A$). The trace in the lower panel in Figure 4 shows the events of $\bar{G}(z_C,z_A,t)$ (Figure 2) that were missing

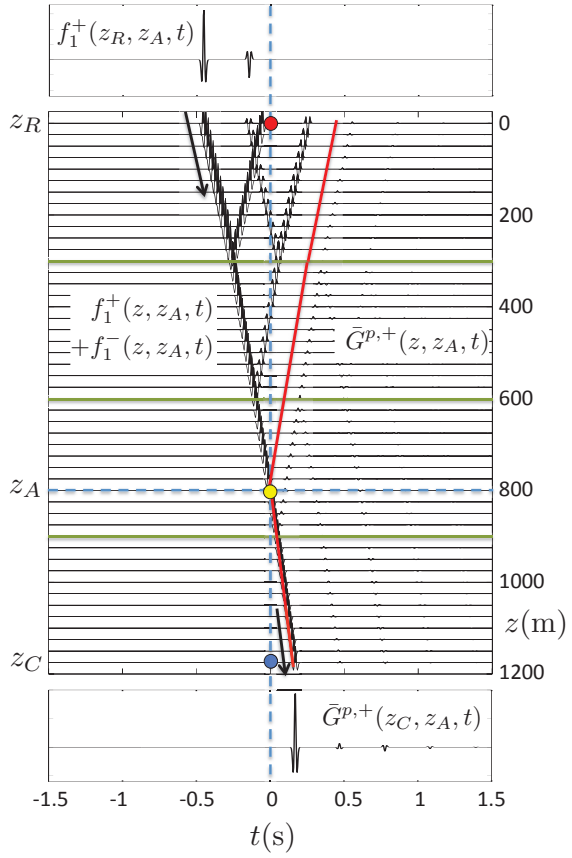


Figure 3: *Response to the focusing function* $f_1^+(z_R,z_A,t)$.

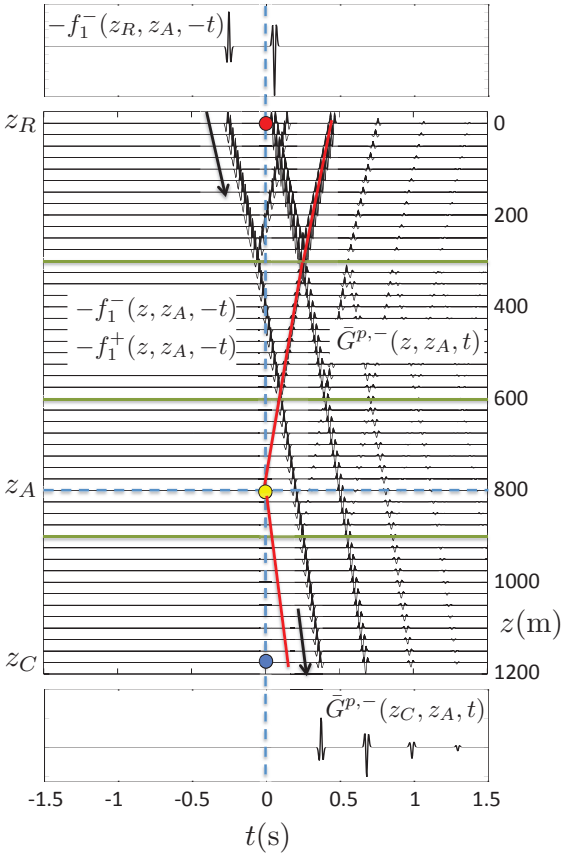


Figure 4: *Response to the focusing function* $-f_1^-(z_R,z_A,-t)$.

in Figure 3. The superposition of Figures 3 and 4 constitutes the desired auxiliary function $\Gamma(z,t)$, because at $z_C$ this gives $\Gamma(z_C,t)=\bar{G}^{p,+}(z_C,z_A,t)+\bar{G}^{p,-}(z_C,z_A,t)=\bar{G}(z_C,z_A,t)$, see Figure 5. Left of the red lines (and above the yellow dot) the field consists of $H(z_A-z)\{f_1(z,z_A,t)-f_1(z,z_A,-t)\}$, where $H(z)$ is the Heaviside function and $f_1(z,z_A,t)=f_1^+(z,z_A,t)+f_1^-(z,z_A,t)$, and right of the red lines it is $\bar{G}(z,z_A,t)$. Together, this gives

$$\Gamma(z,t)=\bar{G}(z,z_A,t)+H(z_A-z)\{f_1(z,z_A,t)-f_1(z,z_A,-t)\}. \tag{5}$$

Hence, by subtracting $\Gamma(z,t)$ from $\bar{G}(z,z_A,t)$, i.e., $\bar{G}(z,z_A,t)-\Gamma(z,t)$ (Figure 6), we are left with the focusing function and its time-reversal above $z_A$ (the yellow dot). The field in the half-space below the yellow dot is zero, hence also its vertical derivative is zero, so the Dirichlet and Neumann boundary conditions are both obeyed at $z=z_C$.

## SINGLE-SIDED REPRESENTATIONS

Following a more formal 3D derivation in the space-frequency domain, we obtain analogous to (5)

$$\Gamma(\mathbf{x},\omega)=\bar{G}(\mathbf{x},\mathbf{x}_A,\omega)+H(z_A-z)2j\Im\{f_1(\mathbf{x},\mathbf{x}_A,\omega)\}, \tag{6}$$

where $\Im$ denotes the imaginary part (Wapenaar et al., 2016). Substitution into equation (4), taking the real part of both sides, and using $2\Re\{G(\mathbf{x},\mathbf{x}_B,\omega)\}=G_\mathrm{h}(\mathbf{x},\mathbf{x}_B,\omega)$, gives

$$G_\mathrm{h}(\mathbf{x}_A,\mathbf{x}_B,\omega)=\int_{\partial\mathbb{D}_R}\frac{2}{\omega\rho(\mathbf{x})}\Big(\Im\{f_1(\mathbf{x},\mathbf{x}_A,\omega)\}\partial_3 G_\mathrm{h}(\mathbf{x},\mathbf{x}_B,\omega) -\Im\{\partial_3 f_1(\mathbf{x},\mathbf{x}_A,\omega)\}G_\mathrm{h}(\mathbf{x},\mathbf{x}_B,\omega)\Big)\mathrm{d}^2\mathbf{x}, \tag{7}$$

see Figure 7. Note that the Green's function $G_\mathrm{h}(\mathbf{x},\mathbf{x}_B,\omega)$ under the integral can be obtained from a similar representation. With some simple replacements (and using source-receiver reciprocity) we obtain

$$G_\mathrm{h}(\mathbf{x},\mathbf{x}_B,\omega)=\int_{\partial\mathbb{D}_S}\frac{2}{\omega\rho(\mathbf{x}')}\Big(\Im\{f_1(\mathbf{x}',\mathbf{x}_B,\omega)\}\partial'_3 G_\mathrm{h}(\mathbf{x},\mathbf{x}',\omega) -\Im\{\partial'_3 f_1(\mathbf{x}',\mathbf{x}_B,\omega)\}G_\mathrm{h}(\mathbf{x},\mathbf{x}',\omega)\Big)\mathrm{d}^2\mathbf{x}', \tag{8}$$

with $\mathbf{x}$ on $\partial\mathbb{D}_R$ and $\mathbf{x}'$ on $\partial\mathbb{D}_S$, just above $\partial\mathbb{D}_R$. Note that $G_\mathrm{h}(\mathbf{x},\mathbf{x}',\omega)$ stands for the reflection response at the surface. Hence, equations (7) and (8) can be used to retrieve the homogeneous Green's function $G_\mathrm{h}(\mathbf{x}_A,\mathbf{x}_B,\omega)$ from the reflection response $G_\mathrm{h}(\mathbf{x},\mathbf{x}',\omega)$. This two-step process is summarised as

$$G_\mathrm{h}(\mathbf{x},\mathbf{x}',\omega)\xrightarrow{f_1(\mathbf{x}',\mathbf{x}_B,\omega)}G_\mathrm{h}(\mathbf{x},\mathbf{x}_B,\omega)\xrightarrow{f_1(\mathbf{x},\mathbf{x}_A,\omega)}G_\mathrm{h}(\mathbf{x}_A,\mathbf{x}_B,\omega). \tag{9}$$

This is similar to standard pre-stack redatuming (Berkhout, 1982; Berryhill, 1984), except that here all multiple reflections (including surface-related multiples (Singh et al., 2015)) are properly handled.

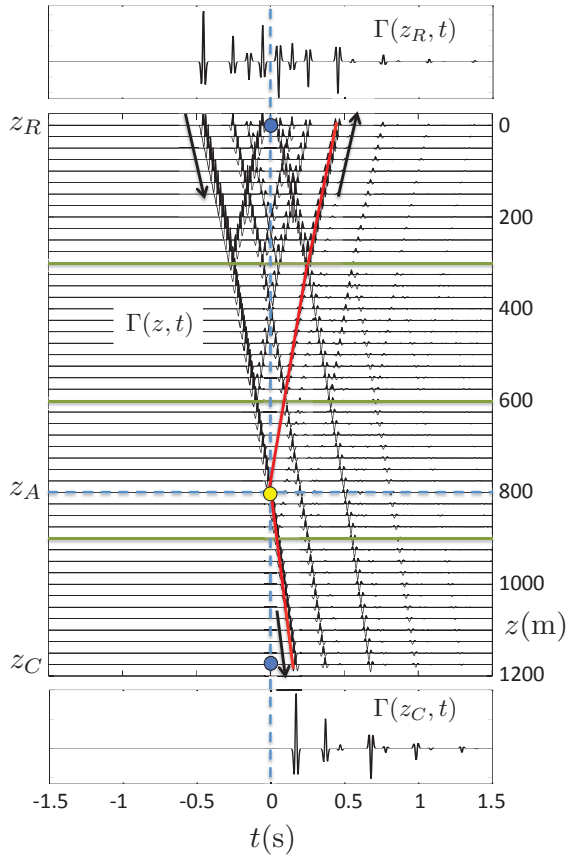


Figure 5: *The auxiliary function $\Gamma(z,t)$, consisting of the superposition of Figures 3 and 4.*

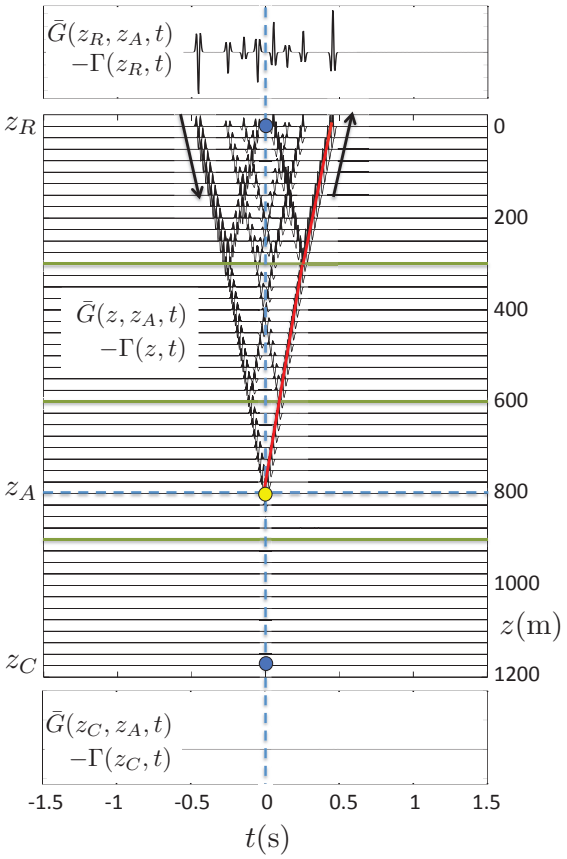


Figure 6: *The difference function $\bar{G}(z,z_A,t)-\Gamma(z,t)$, which obeys the Cauchy boundary condition at $z_C$.*

## CONCLUSIONS

Starting with the classical homogeneous Green's function representation for the configuration of Figure 1(a) (equation 1), we modified the configuration to two parallel boundaries $\partial\mathbb{D}_R$ and $\partial\mathbb{D}_C$ (Figure 1(b)), and discussed a way to eliminate the integral along the lower boundary $\partial\mathbb{D}_C$. To this end we introduced an auxiliary function, which consists of focusing functions, emitted from the upper boundary, which reproduce the Green's function at the lower boundary. Hence, by subtracting this auxiliary function from the Green's function, the integral along the lower boundary vanishes, leaving a single-sided representation of the homogeneous Green's function (Figure 7).

Note that the focusing functions appearing in the single-sided representation are those we derived earlier for Marchenko imaging. These focusing functions can be retrieved from the reflection response at the surface and an estimate of the direct arrival between the focal point and the surface. Hence, the two-step redatuming process, summarised by equation (9), handles multiple reflections in a data-driven way. Apart from imaging, we foresee interesting applications of the single-sided homogeneous Green's function representation in inverse scattering, time-reversal acoustics, seismic interferometry, passive source imaging, etc.

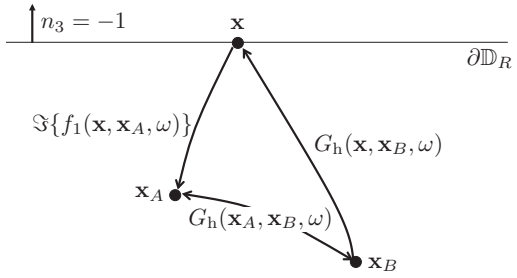


Figure 7: *Visualisation of the single-sided homogeneous Green's function representation (equation 7). Similar as in Figure 1, the rays represent the full responses between the source and receiver points, including multiple scattering.*

## REFERENCES


Berkhout, A. J., 1982, Seismic Migration. Imaging of acoustic energy by wave field extrapolation. A. Theoretical aspects: Elsevier.

Berryhill, J. R., 1984, Wave-equation datuming before stack: Geophysics, **49**, 2064–2066.

Broggini, F., and R. Snieder, 2012, Connection of scattering principles: a visual and mathematical tour: European Journal of Physics, **33**, 593–613.

Derode, A., E. Larose, M. Campillo, and M. Fink, 2003, How to estimate the Green's function of a heterogeneous medium between two passive sensors? Application to acoustic waves: Applied Physics Letters, **83**, 3054–3056.

Esmersoy, C., and M. Oristaglio, 1988, Reverse-time wave-field extrapolation, imaging, and inversion: Geophysics, **53**, 920–931.

Fink, M., 1997, Time reversed acoustics: Physics Today, **50**, 34–40.

———, 2008, Time-reversal acoustics: Journal of Physics: Conference Series, **118**, 012001.

Lindsey, C., and D. C. Braun, 2004, Principles of seismic holography for diagnostics of the shallow subphotosphere: The Astrophysical Journal Supplement Series, **155**, 209–225.

Maynard, J. D., E. G. Williams, and Y. Lee, 1985, Nearfield acoustic holography: I. Theory of generalized holography and the development of NAH: Journal of the Acoustical Society of America, **78**, 1395–1413.

McMechan, G. A., 1983, Migration by extrapolation of time-dependent boundary values: Geophysical Prospecting, **31**, 413–420.

Morse, P. M., and H. Feshbach, 1953, Methods of theoretical physics, Vol. I: McGraw-Hill Book Company Inc., New York.

Oristaglio, M. L., 1989, An inverse scattering formula that uses all the data: Inverse Problems, **5**, 1097–1105.

Porter, R. P., 1970, Diffraction-limited, scalar image formation with holograms of arbitrary shape: Journal of the Optical Society of America, **60**, 1051–1059.

Porter, R. P., and A. J. Devaney, 1982, Holography and the inverse source problem: Journal of the Optical Society of America, **72**, 327–330.

Singh, S., R. Snieder, J. Behura, J. van der Neut, K. Wapenaar, and E. Slob, 2015, Marchenko imaging: Imaging with primaries, internal multiples, and free-surface multiples: Geophysics, **80**, S165–S174.

Slob, E., K. Wapenaar, F. Broggini, and R. Snieder, 2014, Seismic reflector imaging using internal multiples with Marchenko-type equations: Geophysics, **79**, S63–S76.

van der Neut, J., K. Wapenaar, J. Thorbecke, E. Slob, and I. Vasconcelos, 2015, An illustration of adaptive Marchenko imaging: The Leading Edge, **34**, 818–822.

Wapenaar, K., 2003, Synthesis of an inhomogeneous medium from its acoustic transmission response: Geophysics, **68**, 1756–1759.

Wapenaar, K., F. Broggini, E. Slob, and R. Snieder, 2013, Three-dimensional single-sided Marchenko inverse scattering, data-driven focusing, Green's function retrieval, and their mutual relations: Physical Review Letters, **110**, 084301.

Wapenaar, K., J. Fokkema, and R. Snieder, 2005, Retrieving the Green's function in an open system by cross-correlation: a comparison of approaches (L): Journal of the Acoustical Society of America, **118**, 2783–2786.

Wapenaar, K., J. Thorbecke, and J. van der Neut, 2016, A single-sided homogeneous Green's function representation for holographic imaging, inverse scattering, time-reversal acoustics and interferometric Green's function retrieval: Geophysical Journal International, **205**, 531–535.

Weaver, R. L., and O. I. Lobkis, 2004, Diffuse fields in open systems and the emergence of the Green's function (L): Journal of the Acoustical Society of America, **116**, 2731–2734.

Weglein, A. B., R. H. Stolt, and J. D. Mayhan, 2011, Reverse time migration and Green's theorem: Part II - A new and consistent theory that progresses and corrects current RTM concepts and methods: Journal of Seismic Exploration, **20**, 135–159.

Wu, R. S., and M. Toksöz, 1987, Diffraction tomography and multisource holography applied to seismic imaging: Geophysics, **52**, 11–25.